



Application of high-resolution transmission electron microscopy and electron energy-loss spectroscopy in the characterization of polymer nanotubes

Lei Shang, Xiaoru Li, Yiqian Wang*

*The Cultivation Base for State Key Laboratory, Qingdao University, No. 308 Ningxia Road, Qingdao, 266071, P.R. China; fax: +86 532 8378 0318; e-mail: yqwang@qdu.edu.cn

(Received: 13 July, 2012; published: 03 March, 2013)

Abstract: Polyamide 6 (PA6) and polystyrene (PS) nanotubes were successfully fabricated by polymer solution-wetting method. High-resolution transmission electron microscopy (HRTEM), X-ray diffraction (XRD) and electron energy-loss spectroscopy (EELS) techniques were employed to investigate their crystallization phenomena. It has been found in HRTEM images that the crystalline lattice fringes are observed in some regions of the nanotube walls. XRD analysis showed that these two kinds of polymer nanotubes have a higher degree of crystallinity than that of the bulk materials. PA6 nanotubes dominate in γ phase while bulk PA6 present mainly in α phase. EELS has been used to determine the ratio of C=C and C-C in PS nanotubes, and our result is consistent with the theoretical calculation. HRTEM and EELS will shed light on the microstructural characterization of polymer nanotubes.

Keywords: PA6 nanotube, PS nanotube, HRTEM, EELS, XRD

Introduction

In recent years, polymer nanostructures have attracted considerable attention due to their unique properties and potential applications in a variety of areas, such as nanoelectronic devices, ultrafiltration, catalysis, medicine, transport, separation, and sensors [1-6].

As we all know, microstructure determines properties of materials. So it is important to explore the microstructure of the polymers especially for nanomaterials. Nowadays, many methods can be used to study the microstructure of polymers, such as polarization microscope (PLM), atomic force microscope (AFM), scanning electron microscope (SEM), small-angle X-ray scattering (SAXS), and high-resolution transmission electron microscopy (HRTEM). But all of these methods have their own limitations. SAXS has become one of the most useful techniques for structural investigation of semicrystalline polymers and it can be used to determine either the micro or nano-scale structure of particle systems in terms of parameters such as average particle sizes, shapes, distribution, and surface-to-volume ratio [7-13]. PLM can be used to observe the morphology of polymers, however, its resolution is much lower than that of HRTEM. As one of the characterization techniques, HRTEM has been used successfully to study intermetallic compounds [14] and metallic carbides [15], oxides [16] and most recently metals [17], but it is difficult to use HRTEM for the study of organic molecules and polymers. The main problem is that organic molecules suffer irradiation damage from the incident electron beam during the examination and this severely limits the resolution that can be attained [18]. Electron

energy-loss spectroscopy (EELS) is a very powerful technique and can be used to measure the spectrum of electronic excitations in various materials, both crystalline and amorphous. It has been widely used in chemical microanalysis, studies of solid state effects and successfully applied to the determination of the electronic structure [19, 20]. However, to our knowledge, only few reports can be found, concerning the application of HRTEM and EELS in the microstructure characterization of polymer nanotubes.

In this paper, we report a detailed microstructure investigation of polyamide 6 (PA6) and polystyrene (PS) nanotube obtained by anodic aluminum oxide (AAO) template synthesis by polymer solution-wetting [21, 22]. Crystalline behaviors of PA6 nanotube and PS nanotube were investigated using HRTEM. The change of crystalline form was studied by X-ray diffraction (XRD). EELS has been used to determine the ratio of C=C and C-C in PS nanotube at room temperature.

Results and Discussion

Morphology and microstructure of PA6 and PS nanotubes

-PA6 nanotubes

Figure 1(a) is a SEM image of PA6 nanotubes. It shows typical PA6 nanotube arrays. From Figure 1(a), PA6 nanotubes with an outer diameter of 300 nm can be clearly observed. In addition, the length of PA6 nanotubes is not uniform.

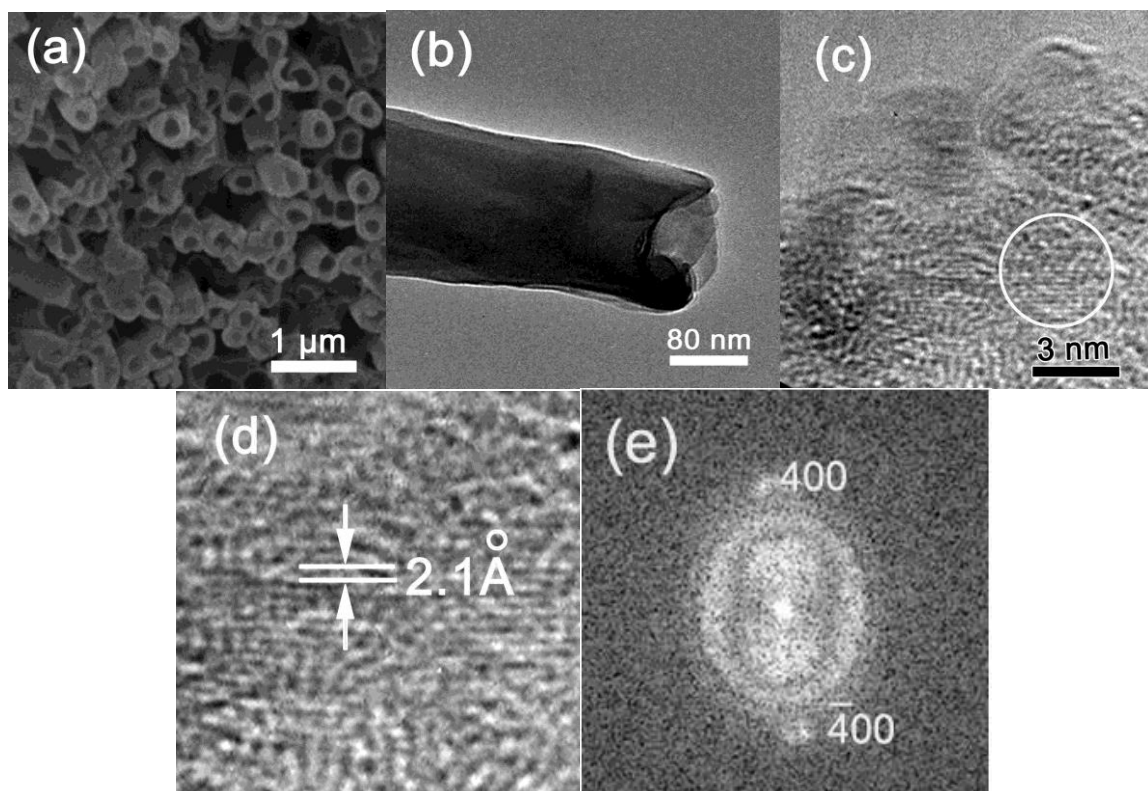


Fig. 1. (a) SEM images of the PA6 nanotube arrays; (b) a typical TEM image of PA6 nanotube; (c) HRTEM image of the sidewall in image (b); (d) enlarged view of marked area in (c); (e) FFT image of (c).

This is related to processing method. The pores of AAO template have different diameter and length, so the volume of every pore is different. When the polymer solution permeates into the pores, it forms nanotubes according to the length of the pores. Thus, nanotubes of different length may form. The other reason is that while preparing polymer nanotubes, a solution of about 5 μL was dropped on to microscope glass to obtain hollow nanotubes which can be observed clearly. However, five-microliter solution only wets the template partially, so some pores do not have adequate solution to cover the pores completely. Hence, nanotubes shorter than the length of pores were produced. [23]

Figure 1(b) shows a typical TEM image of PA6 nanotube. A continuous hollow space inside is clearly visible.

Figure 1(c) presents a typical HRTEM image of the side wall of PA6 (nylon) nanotube. It is well known that nylon has a higher degree of crystallinity than other polymers, and it is a typical semicrystalline polymer. We can see clearly from this image that crystalline lattice fringes exist in some regions while most regions show an amorphous nature. The lattice spacing is measured to be 0.21 nm from enlarged HRTEM image in Figure 1(d). This distance is close to the (400) planar spacing ($d_{400}=2.02 \text{ \AA}$) of PA6 nanotube.

It can be seen from the FFT of the HRTEM image in Figure 1(e) that there are two distinct diffraction spots, which can be indexed as (400) and $(\bar{4}00)$ respectively. The two diffuse rings indicate that there are amorphous regions in the PA6 nanotubes.

-PS nanotubes

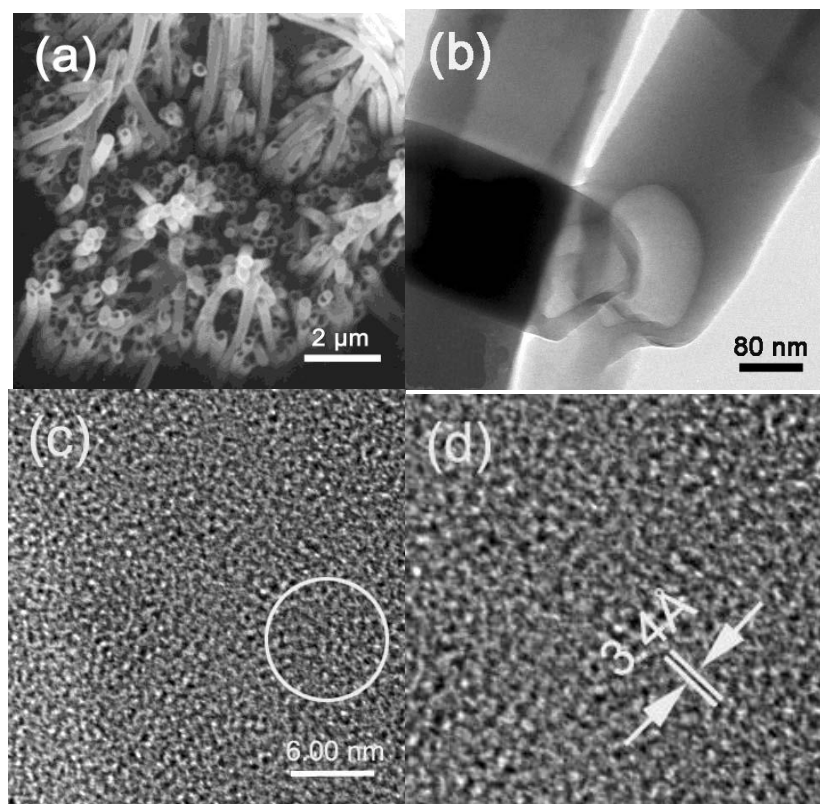


Fig. 2. (a) SEM image of PS nanotube arrays; (b) TEM image of PS nanotubes; (c) HRTEM image of the sidewall in image (b); (d) enlarged view of marked area in (c).

It is well known that polystyrene has a low degree of crystallinity. The morphology and microstructure of PS nanotubes is confirmed by SEM and TEM in Figure 2. Figure 2(a) shows a SEM image of PS nanotube arrays. In Figure 2(a), the enlarged top view of PS nanotubes shows open mouth. Careful examination of Figure 2(a) shows that some mouths are plain, while the others are oblique. The length of PS nanotubes is not even. In Figure 2(b), the hollow of the PS nanotubes can be seen. Some walls are thick and the others are thin. The non-uniformity of wall thickness for PS nanotubes in Figure 2(a) is attributed to the different morphology of inner walls and also possibly due to the concentration gradient of solution on the surface liquid drop. This phenomenon can be seen clearly in Figure 2(b).

Figure 2(c) presents a typical HRTEM image of the side wall of PS nanotube. We can see from this image that crystalline lattice fringes exist in some regions and the lattice spacing is measured to be 3.4 Å (Figure 2(d)), while most regions show an amorphous nature.

XRD of PA6 and PS nanotubes

-PA6 nanotubes

XRD analysis was performed to investigate the crystal structure and orientation difference between PA6 nanotubes and bulk PA6. Figure 3(a) is an XRD profile taken from bulk PA6. The XRD profile taken from PA6 nanotube is shown in Figure 3(b).

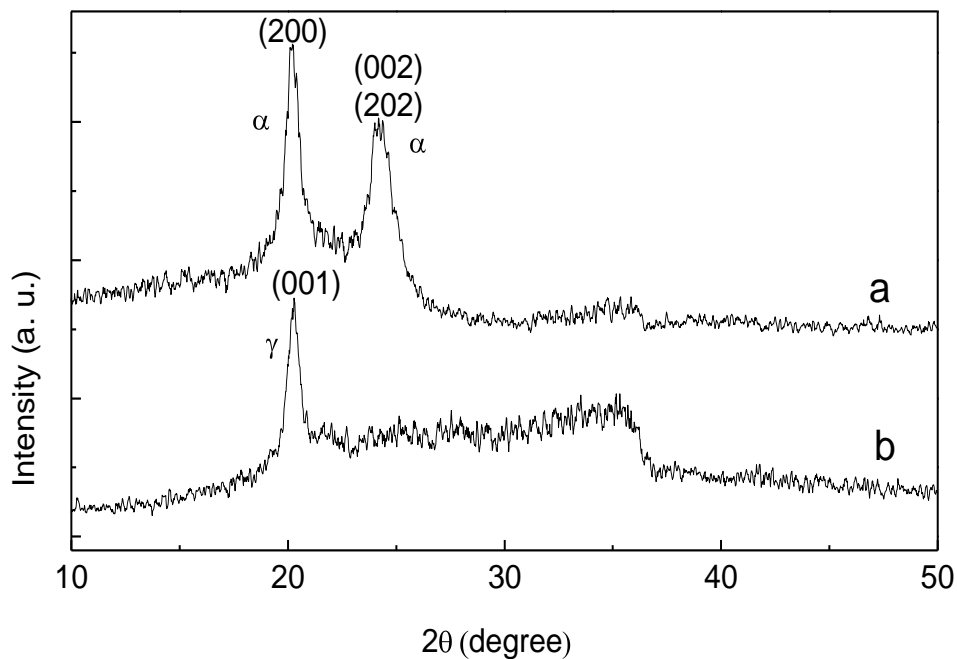


Fig. 3. XRD spectra of polyamide 6: (a) bulk PA6; (b) PA6 nanotubes.

It was reported [24,25] that for bulk PA6 two main reflections at 20° and 24° were attributed to α-form crystal and the reflection at about 21° corresponds to the γ-form crystal. From Figure 3, it can be seen that there are two major peaks at 20.33° and 24.22° for bulk PA6, while only one peak at 20.28° for PA6 nanotube. So it can be concluded that for bulk PA6 exhibits α-form crystals whereas PA6 nanotubes only

has γ structure. Additionally, it can be seen that PA6 nanotube has a higher degree of crystallinity than bulk PA6 because the peak at 20.28° is narrower than the other peaks for the bulk PA6.

For bulk PA6, two reflection peaks at 20.33° and 24.22° are corresponding to lattice space 4.37 \AA and 3.68 \AA , respectively. The crystalline orientation $\alpha(200)$ and $\alpha(002)/(202)$ is preferential. Whereas PA6 nanotubes (Figure 3(b)) only one reflection peak at $2\theta = 20.23^\circ$ related to the γ -form crystal. According to Bragg equation, the corresponding lattice spacing is 4.38 \AA , which is consistent with our HRTEM observation. The dominating crystalline orientation is $\gamma(001)$.

Although the crystal properties of polymers are influenced by processing conditions, the main factor affecting the occurrence of the γ structure in PA6 nanotubes was the presence of nanopores during growth.

The unit cells of α and γ phases are different, the unit cell for α is characterized by $a=9.56 \text{ \AA}$, $b=17.24 \text{ \AA}$, $c=8.01 \text{ \AA}$, $\alpha=\gamma=90^\circ$, $\beta=67.5^\circ$ [26]; and the unit cell for γ by $a=9.33 \text{ \AA}$, $b=16.88 \text{ \AA}$, $c=4.78 \text{ \AA}$, $\alpha=\gamma=90^\circ$, $\beta=121^\circ$ [27]. Therefore, the two most intense reflections of the α and γ phases appear at slightly different angles and are at, $20^\circ(200, \alpha1)/24^\circ(002+202, \alpha2)$, and $22^\circ(001, \gamma1) / 23^\circ(201+200, \gamma2)$ respectively.

-PS nanotubes

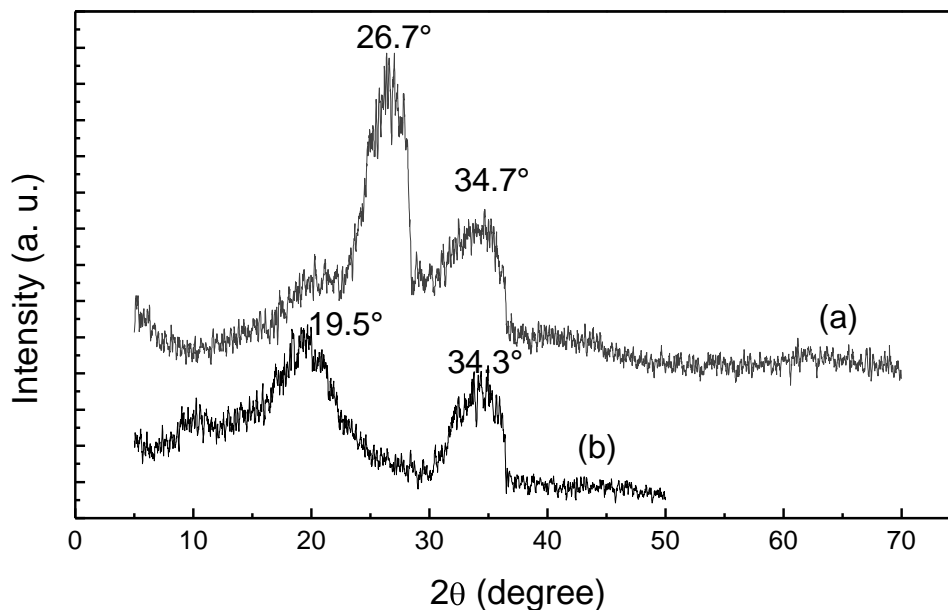


Fig. 4. XRD spectra of polystyrene: (a) PS nanotubes; (b) bulk PS.

XRD analysis was performed to investigate the crystal structure and orientation difference between PS nanotubes and bulk PS. Figure 4 is the XRD profile taken from bulk PS and PS nanotubes. It shows that the curves of bulk PS and PS nanotubes are quite different and the two specimens have different degree of crystallinity. Figure 4(a) is the XRD spectra of PS nanotubes. Figure 4(b) is the XRD spectra of bulk PS. It can be seen that both PS nanotube and bulk PS, there are two major peaks, bulk PS at 19.5° and 34.3° while PS nanotube at 26.7° and 34.7° . Thus it can be seen that the lattice space of PS nanotube is smaller than that of bulk PS. According to Bragg equation, the corresponding lattice spacings are 3.34 \AA and 2.59 \AA for PS nanotube which are consistent with our HRTEM measurement. It can be

seen that PS nanotubes have a higher degree of crystallinity than bulk PS because the peak at 26.7° is narrower than the other peaks for bulk PS.

EELS of PS nanotubes

Figure 5 shows a typical EELS spectrum of the carbon K-edge for PS nanotubes at room temperature. For the chemical characterization of PS nanotubes, we focused on the carbon K-edges. Several features in the fine structure can be distinguished. The electron-energy loss near-edge fine structure (ELNES) is composed of transitions first from $1s$ towards π^* orbitals and then towards σ^* orbitals. The first peak at 302 eV is assigned to a π^* orbital while the second one at 346 eV is assigned to a σ^* orbital.

After the background subtraction and deconvolution of the EELS spectrum, the π^*/σ^* intensity ratio is calculated to be 0.47. In fact, the molecular ratio of C=C and C-C in PS is 0.5, which is consistent with the ratio calculated from EELS result. So we can draw a conclusion that EELS can be used to investigate the ratio of C=C and C-C in polymer nanostructures.

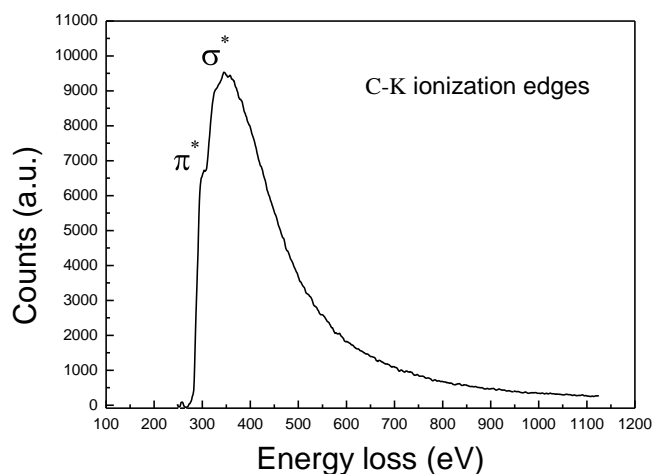


Fig. 5. A typical EELS spectrum taken from one of PS nanotubes.

Conclusions

In summary, using the mini-dose operation, HRTEM can be successfully used to analyze the morphology of polymers. HRTEM images can show the lattice fringes in some regions of PA6 and PS nanotubes. XRD analysis indicates that PA6 and PS nanotubes have a higher degree of crystallinity than in their bulk forms. PA6 nanotube is composed of mostly γ phase, and bulk PA6 consists of predominantly α phase. EELS is successfully applied for the determination of C=C and C-C ratios. Combination of HRTEM and EELS will shed light on the microstructure of polymer nanostructures.

Experimental

Preparation of PA6 and PS nanotubes

The AAO template (from Whatman International Ltd.) has pore diameter ranging from 150 to 300 nm and the length ranging from 50 to 60 μm . It was treated with alcohol in

an ultrasonic bath to clean its surface before use. PA6 and PS nanotubes were prepared by solution-wetting method.

Preparation of PA6 nanotubes

PA6 was first solved in formic acid to prepare a 4.0 wt.% solution. Next, a small amount of solution was put on top of a clean glass slide. Then an AAO membrane was placed onto the solution within a few seconds. The solution will permeate completely into the template pores along their inner walls in 2 seconds. After 1-2 minutes, the solvent will also evaporate completely. The resultant AAO/PA6 composite membrane was then removed from the microscope slide by soaking in hot water and then placed in a 3 M sodium hydroxide solution to dissolve the template. Finally, PA6 nanotubes were obtained.

Preparation of PS nanotubes

The procedure for PS nanotube preparation is similar to that of PA6 nanotube except different solution formation is used. In PS nanotube formation, PS was first dissolved in trichloromethane to achieve a 2.5 wt.% solution rather than a 4.0 wt.% PA6 solution. The rest of the procedure is the same as the preparation of PA6 nanotubes.

Characterization of PA6 and PS nanotubes

The morphology of PA6 and PS nanostructure arrays was investigated using a JEOL JSM-6390LV SEM. PA6 and PS nanotubes were sputtered with 10 nm of Au prior to SEM (JEOL JSM-840) imaging. The microstructure of PA6 and PS nanotubes was studied using a Philips CM200-FEG transmission electron microscope. XRD analysis was performed on a **Bruker** D8 Advance with a Cu K α radiation ($\lambda=1.5418 \text{ \AA}$).

TEM examinations were conducted under conditions of mini-dose operation to minimize radiation damage in order to increase observation time under the electron microscope before the sample is damaged. The specimen for TEM observation was prepared by evaporating a 5 μL drop of the nanostructure dispersion onto a carbon-film-coated copper grid.

Acknowledgements

The authors would like to thank the financial support from National Key Basic Research Development Program of China (973 special preliminary study plan) (Grant no.: 2012CB722705), the Natural Science Foundation for Outstanding Young Scientists in Shandong Province (Grant no.: JQ201002), the Scientific Research Award for Outstanding Young and Middle-Aged Scientists in Shandong Province (Grant no.: BS2009CL0005), the Program of Science and Technology for Higher Education in Shandong Province (Grant no.: J12LA17), and the Scientific Research Starting Foundation for Introduced Talents at Qingdao University (Grant no.: 06300701). One author (Y.Q. Wang) would also like to thank the financial support from Taishan Scholar Program (Outstanding Overseas Scholar) of Shandong Province.

References

- [1] Bong, D. T.; Clark, T. D.; Granja, J. R.; and Ghadiri, M. R. *Angew. Chem. Int. Ed.* **2001**, *40*, 988.
- [2] MacDiarmid, A. G. *Angew. Chem. Int. Ed.* **2001**, *40*, 2581.

- [3] Tan, E. P. S. and Lim, C. T. *Appl. Phys. Lett.* **2004**, *84*, 1603.
- [4] Steinhart, M.; Wehrspohn, R. B.; Gösele, U.; Wendorff, J. H. *Angew. Chem. Int. Ed.* **2004**, *43*, 1334.
- [5] Danginet-De, Pra L.; and Demoustier-Champagne, S. *Polymer* **2005**, *46*, 1583.
- [6] Wang, C. C.; Kei, C. C.; Yu, Y. W.; Perng, T. P. *Nano Lett.* **2007**, *7*, 1566.
- [7] Balta-Calleja, F. J.; Vonk, C. G.; Jenkins, A. D. (ed.) *Amsterdam: Elsevier*, **1989**, 241.
- [8] Guinier, A.; Fournet, G. New York (London), Wiley (Chapman and Hall), **1955**.
- [9] Glatter, O.; Kratky, O. New York, Academic Press, **1982**.
- [10] Martin, C.; Eeckhaut, G.; Mahendrasingam, A.; *et al.* *J Synchrotron Rad.* **2000**, *7*, 245.
- [11] Creagh, D. C.; O'Neill, P. M.; Martin, D. J. *J Synchrotron Rad.* **1997**, *4*, 163.
- [12] Goertz, V.; Dingenouts, N.; Nirschl, H. *Part. Part. Syst. Character.* **2009**, *26*, 17.
- [13] Campoy, I.; Go´mez, M. A.; Marco, C. *Polymer* **2000**, *41*, 2295.
- [14] Tendeloo, G. V. *J. Microsc.* **1980**, *119*, 125.
- [15] Jepps, N. W. and Page, T. F. *J. Microsc.* **1980**, *119*, 177.
- [16] Bursill, L. A. and Wood, G. J. *Phil. Mag. A.* **1978**, *38*, 673.
- [17] Cosslett, V. E.; Camps, R. A.; Saxton, W. O.; *et al.* *Nature* **1979**, *281*, 49.
- [18] Read, R. T.; Young, R. J. *J. Mater. Sci.* **1984**, *19*, 327.
- [19] Egerton, R. F. New York, Plenum Press, **1996**.
- [20] Varlot, K.; Martin, J. M.; Quet C. *Micron* **2001**, *32*, 371.
- [21] Song, G. J.; She, X. L.; Fu, Z. F.; and Li, J. J. *J. Mater. Res.* **2004**, *19*, 3324.
- [22] Li, J. J.; Song, G. J.; She, X. L. *Polym. J.* **2006**, *38*, 554.
- [23] She, X. L.; Song, G. J.; *et al.* *J. Mater. Res.* **2006**, *21*, 1209.
- [24] Campoy, I.; Gómez, M. A.; Marco, C. *Polymer* **1998**, *39*, 6279.
- [25] Ramesh, C. and Bhoje, G. E. *Macromolecules*, **2001**, *34*, 3308.
- [26] Holmes, D. R.; Bunn, C. W.; Smith, D. J. *J. Polym. Sci.* **1955**, *17*, 159.
- [27] Arimoto, H.; Ishibashi, M.; Hirai, M.; Chatani, Y. *J. Polym. Sci.* **1965**, *3*, 317.